Volume 22
Number 30
5 August 2026
Pages 4971–5128

Soft Matter

rsc.li/soft-matter-journal

ISSN 1744-6848

ROYAL SOCIETY
OF CHEMISTRY

PAPER
Francisca Guzmán-Lastra *et al.*
Dynamics of magnetic self-propelled particles in a harmonic trap

Soft Matter

PAPER

Published on 08 June 2026
Licence and permissions

Check for updates

Cite this: *Soft Matter*, 2026, **22**, 4994

Dynamics of magnetic self-propelled particles in a harmonic trap

Pamela Muñoz-Obreque,[a] Oscar Garrido,[b] Erick Burgos-Parra,[b] Diego Romero,[b] Hartmut Löwen[c] and Francisca Guzmán-Lastra*[b]

Received 27th April 2026, Accepted 3rd June 2026

DOI: 10.1039/d6sm00387g

rsc.li/soft-matter-journal

Artificial active particles provide a powerful platform to investigate non-equilibrium collective behavior. Here, we use Hexbugs equipped with embedded magnetic dipoles as macroscopic realizations of magnetic self-propelled particles (MSPPs) to study active matter under confinement. By combining experiments and simulations, we analyze their dynamics within a parabolic domain modeled as a symmetric external harmonic potential. We uncover a rich landscape of metastable and dynamically evolving configurations, including climbing chains, polarized orbiting clusters, and rotating ring-like states, arising from the competition between dipolar interactions, confinement, and activity. While orbiting states are recovered at the single-particle level, we show that self-alignment alone does not determine the collective dynamics, which instead emerge from magnetic interactions. We demonstrate that the number of particles and the relative strength of magnetic interactions and harmonic confinement control the structure and stability of these states. Our experimental observations are quantitatively reproduced by a minimal model of disk-like magnetic active Brownian particles with inertial translational dynamics and overdamped orientation. These results provide a unified framework for understanding structure formation and dynamical states in confined active systems with dipolar interactions.

I. Introduction

In recent decades, the study of active Brownian particles (ABPs) has attracted considerable attention due to their intrinsically non-equilibrium nature. Unlike passive Brownian particles, which rely solely on thermal fluctuations, ABPs are either equipped with an internal motor or continuously extract energy from their surroundings to sustain persistent motion and out-of-equilibrium states.[1–3] This property gives rise to rich individual and collective behaviors,[4] making ABPs a central paradigm in Active Matter.[2,5–8] These systems provide a unifying framework to study emergent phenomena across a wide range of scales, from biological systems such as bird flocks, fish schools, and bacterial colonies,[9,10] to synthetic realizations including microrobots and colloidal particles.[11–14]

A defining feature of active matter is its strong sensitivity to confinement.[12,15–19] In confined geometries, persistent motion leads to particle accumulation near boundaries and to non-uniform density distributions.[12,15,16,20] A particularly relevant realization is confinement in harmonic (parabolic) potentials, where rotational symmetry is preserved and single-particle dynamics organize around a characteristic radius set by the balance between propulsion and restoring forces.[21,22] In this setting, active particles can display radially polarized (climbing) states or circular motion when self-alignment is present.[23–26] At finite densities, a broader range of behaviors emerges, including polar organization[27,28] and Boltzmann-like distributions that depend sensitively on the balance between activity and trap strength.[29,30]

In contrast, anisotropic confinement, such as elliptic geometries, breaks rotational symmetry and introduces spatial heterogeneity in curvature and restoring forces. This leads to anisotropic trajectories, position-dependent velocities, and new dynamical regimes including deformed limit cycles and directional transport.[25,26,31] Confinement therefore acts not only as a geometric constraint, but also as a control parameter that selects and stabilizes distinct dynamical states.

Recent studies have shown that confinement alone can induce non-trivial collective states even in the absence of explicit self-alignment mechanisms. For instance, Aranson *et al.*[31] demonstrated that active particles in asymmetric parabolic traps can form orbiting condensates with crystalline order, where particle velocities align with the local potential gradient. In the context of inertial active particles, Gutirrez *et al.*[30] showed that particles exhibit climbing states under weak confinement and condense near the trap center when confinement is strong.

[a] *Departamento de Física, Facultad de Ciencias, Universidad de Santiago de Chile, Santiago, Chile*

[b] *Departamento de Física, Facultad de Ciencias, Universidad de Chile, Santiago, Chile. E-mail: fguzman@uchile.cl*

[c] *Institut für Theoretische Physik II: Weiche Materie, Heinrich-Heine-Universität Düsseldorf, D-40225 Düsseldorf, Germany*

These results indicate that confinement and interactions can generate structured collective states without the need for explicit self-alignment.

A particularly important interaction in both natural and artificial systems is the magnetic dipole–dipole interaction.[32] In natural systems, such as magnetotactic bacteria, experiments have revealed bioconvection patterns and vortex dynamics under the action of external magnetic fields.[33–37] In synthetic systems, dipolar microswimmers provide a platform to control particle motion and collective behavior, with promising applications in biomedical contexts.[33,38–40] In these systems, particles interact *via* long-range dipolar forces, enabling the formation of structured assemblies and complex dynamical states even in the absence of external fields.[41–44] Magnetic interactions lead to alignment, but the alignment behavior is anisotropic and, therefore, different from the isotropic alignment typically assumed in Viscek-like models.[45]

At high particle concentrations, the interplay between activity and dipolar interactions leads to transient metastable states and continuous reorganization, resulting in complex collective dynamics,[41,43,46] which have also been experimentally observed in the presence of imbalanced interactions.[47] In contrast, when the number of particles is small, the system exhibits a limited set of configurations that strongly depend on particle number. In this regime, both experiments and simulations have reported the formation of chains and ring-like structures, with particles dynamically reconfiguring between these states.[48,49] For instance, T'elezki *et al.*[43] showed that even in circular confinement, a small number of magnetic self-propelled particles can form chains and rotating ring-like configurations.

Despite these advances, the behavior of small groups of interacting magnetic active particles under confinement remains poorly understood. This raises a fundamental question: what mechanisms govern the emergence and stability of collective states in confined systems with only a few interacting particles? In particular, it is unclear how the competition between activity, dipolar interactions, and harmonic confinement determines the structure and dynamics of these systems. While dipolar interactions tend to promote ordered, low-energy configurations, activity drives the system out of equilibrium, leading to persistent reorganization. Understanding how these competing effects shape the dynamics and stability of configurations in confined systems with few particles remains an open question.

Hexbugs (HB), small robots propelled by vibrating motors powered by internal batteries, provide an accessible macroscopic platform to investigate active matter dynamics.[12,23,24,50,51] They exhibit behaviors typical for active particles, including persistent motion and collective organization under confinement.[12,24,51,52] Previous studies have explored their dynamics under different confinement geometries and interaction mechanisms, including elastic, phototactic and magnetic couplings.[11,23,51,53–56]

Here, we investigate the collective dynamics of magnetic self-propelled particles confined in a harmonic potential by combining experiments and numerical simulations. In particular, we focus on the role of dipolar interactions in shaping both steady and dynamically evolving states.

At the single-particle level, we recover orbiting states consistent with previous observations in confined active systems where self-alignment plays a dominant role.[24] However, as the number of particles increases, this behavior is no longer sustained. Instead, the system transitions to a regime where dipolar interactions, together with activity and confinement, dominate the dynamics.

We show that, while a weak self-alignment torque is retained in the model, the collective behavior for $N > 1$ is governed by magnetic-driven effects. In this regime, confinement promotes particle encounters, and dipolar interactions stabilize a rich landscape of metastable and dynamically evolving configurations, including chains, ferromagnetic-like clusters, and rotating structures.

These results demonstrate that, although self-alignment controls single-particle motion, it does not determine the collective behavior of magnetically interacting particles. Instead, the emergence of collective states in confined magnetic active systems is primarily driven by their dipolar interactions, revealing a transition from alignment-dominated single-particle dynamics to interaction-dominated many-body behavior.

II. Magnetic self-propelled particles (MSPP)

We consider a system of N disk-shaped magnetic self-propelled particles (MSPP) confined within a harmonic potential, denoted as U^{HP}. The position of particle i is given by $\mathbf{r}_i(t) = [x_i(t), y_i(t)]$, while its orientation is described by the unit vector $\hat{\mathbf{u}}_i(t) = [\cos\theta_i(t), \sin\theta_i(t)]$ in two dimensions. Each particle carries a magnetic dipole moment $\mathbf{m}_i = m\hat{\mathbf{u}}_i(t)$ aligned with its orientation.

The translational dynamics includes inertia and is governed by

$$M\ddot{\mathbf{r}}_i = F_0\hat{\mathbf{u}}_i(t) - \gamma_{\mathrm{T}}\dot{\mathbf{r}}_i - \nabla_{\mathbf{r}_i}\left(U_i^{\mathrm{HP}} + \sum_{j\neq i}\left(U_{ij}^{\mathrm{WCA}} + U_{ij}^{\mathrm{D}}\right)\right), \quad (1)$$

where M is the particle mass, γ_{T} is the translational friction coefficient, and F_0 is the magnitude of the active force driving the particle along its orientation. This form of inertial active dynamics has been previously used to model Hexbug-like systems.[23]

In contrast, the orientational dynamics is assumed to be overdamped, neglecting rotational inertia. It evolves according to

$$\dot{\hat{\mathbf{u}}}_i = \frac{1}{\gamma_{\mathrm{R}}}\left[\xi_{i,\mathrm{R}}(t) - \mathbf{T}_i + \beta(\hat{\mathbf{u}}_i \times \dot{\mathbf{r}}_i)\right] \times \hat{\mathbf{u}}_i, \quad (2)$$

where γ_{R} is the rotational friction coefficient, and $\xi_{i,\mathrm{R}}(t)$ is a Gaussian white noise with zero mean, $\langle\xi_{i,\mathrm{R}}(t)\rangle = 0$, and correlations $\langle\xi_{i,\mathrm{R}}(t_1)\xi_{j,\mathrm{R}}(t_2)\rangle = D_{\mathrm{R}}\delta(t_1 - t_2)\delta_{ij}$. Here, D_{R} is the rotational diffusion coefficient. The parameter βcontrols the strength of a self-alignment torque that tends to align the particle orientation with its instantaneous velocity. Similar models have been used to describe active particles in harmonic traps.[23,24,27] Each MSPP is subject to three interactions: excluded volume, magnetic dipole–dipole interactions, and harmonic confinement. The excluded volume interaction is modeled by the Weeks–Chandler–Anderson

(WCA) potential

$$U_{ij}^{\mathrm{WCA}} = \begin{cases} 4\varepsilon\left[\left(\dfrac{\sigma}{r_{ij}}\right)^{12} - \left(\dfrac{\sigma}{r_{ij}}\right)^{6}\right], & r_{ij} \le r_{\mathrm{m}} \\ 0, & \text{otherwise} \end{cases} \quad (3)$$

with cutoff $r_{\mathrm{m}} = 2^{1/6}\sigma$ where σ is a softened core diameter.

The magnetic dipole–dipole interaction is given by

$$U_{ij}^{\mathrm{D}} = \frac{\mu_0 m^2}{4\pi r_{ij}^{3}}\left[\hat{\mathbf{u}}_i \cdot \hat{\mathbf{u}}_j - \frac{3(\hat{\mathbf{u}}_i \cdot \mathbf{r}_{ij})(\hat{\mathbf{u}}_j \cdot \mathbf{r}_{ij})}{r_{ij}^{2}}\right], \quad (4)$$

where $\mathbf{r}_{ij} = \mathbf{r}_j - \mathbf{r}_i$ and $r_{ij} = |\mathbf{r}_{ij}|$. The magnetic torque acting on particle i is given by $\boldsymbol{T}_i = \hat{\mathbf{u}}_i \times \nabla_{\hat{\mathbf{u}}_i} U^{\mathrm{D}}$ with $U^D = \sum_{j \ne i} U_{ij}^{D}$ denoting the total magnetic energy.

Finally, the harmonic potential is given by

$$U_i^{\mathrm{HP}} = \frac{\kappa}{2} r_i^{2}, \quad (5)$$

where κ is the trap stiffness and $r_i = |\mathbf{r}_i|$ is the distance from the center of the trap.

A. Numerical simulations

We solve eqn (1) and (2) using standard Brownian dynamics in reduced units. The particle diameter σ, translational friction coefficient γ_{T}, and energy scale ε define the units of length, mass, and energy, respectively. Time is expressed in units of $\tau = \gamma_{\mathrm{T}}\sigma^2/\varepsilon$.

In these reduced units, the translational friction is set to $\gamma_{\mathrm{T}} = 1$, while the rotational friction is fixed to $\gamma_{\mathrm{R}} = 0.04$. The self-alignment strength is taken as $\beta = 0.03$. These parameters are not directly accessible experimentally and are treated as effective phenomenological quantities.

The equations of motion are integrated using a third-order Adams–Bashforth–Moulton predictor–corrector scheme with time step $\Delta t = 10^{-4}\tau$ over a total simulation time $T_{\mathrm{s}} = 10^{4}\tau$.

The system behavior is controlled by three main parameters: the magnetic dipole strength m, the harmonic trap stiffness κ, and the self-alignment strength β. The value of β is calibrated by matching the dynamics of a single MSPP in a harmonic trap between experiments and simulations (see SI and Movie S1).

The experimentally measured values of the magnetic moment m and the harmonic potential strength κ are used as reference parameters. To explore the resulting phase behavior, we vary these quantities over the ranges $m = (10^{-2} - 10^{0})$A m^2 and $\kappa = (10^{-3} - 10^{-1})$N m^{-1}, corresponding to weak and strong dipolar interactions and confinement, respectively. This approach allows us to isolate the role of dipolar interactions and confinement in shaping collective dynamics beyond experimentally accessible regimes.

The dynamics of the system is governed by a set of dimensionless parameters that quantify the competition between activity, dipolar interactions, and confinement. In particular, the ratios $\Lambda_1 = F_0/(\kappa\sigma)$, $\Lambda_2 = \mu_0 m^2/(\kappa\sigma^5)$, and $\Lambda_3 = \mu_0 m^2\gamma_{\mathrm{T}}/(\beta F_0\sigma^3)$ characterize the relative importance of activity *versus* confinement, dipolar interactions *versus* confinement, and dipolar interactions *versus* self-alignment, respectively. These parameters provide a useful framework to interpret the different dynamical regimes observed in the system, as discussed in the following sections.

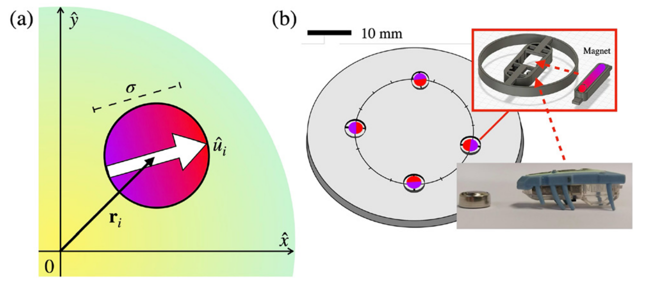

Fig. 1 (a) Schematic of a magnetic self-propelled particle (MSPP) confined in a harmonic potential, defined by its position $\mathbf{r}_i(t)$ and orientation $\hat{\mathbf{u}}_i(t)$. (b) Experimental realization using Hexbug Nano robots equipped with a disk-like armor and embedded magnetic dipole, confined in a parabolic dish.

B. Experiments

We experimentally realize MSPPs using Hexbug Nano robots,[50] equipped with a disk-like armor of diameter $D = 6.5 \pm 0.1$ cm and total mass $M = 18 \pm 0.1$ g. Each particle contains a neodymium rod magnet (diameter 6 ± 0.01 mm, length 3.5 ± 0.1 cm), yielding a magnetic moment $m \approx 0.6$ A m^2.

The particles exhibit persistent motion with average speed $u_0 \approx 3$ cm s^{-1}. Small fluctuations in their orientation are characterized by an effective rotational diffusivity $D_{\mathrm{R}} \sim 10^{-5}$ rad^2 s^{-1}, obtained from trajectory analysis.

The particles are confined within a parabolic surface (satellite dish) of dimensions $L_x = 70$ cm, $L_y = 65$ cm, and $L_z = 5.5$ cm, which generates an effective harmonic trap with stiffness $\kappa = \dfrac{MgL_z}{L_xL_y} \sim 0.01\ \mathrm{N\ m^{-1}}$.

All experimental parameters (M, D, u_0, m, D_{R}, and κ) are independently measured. The remaining parameters in the simulations (γ, γ_{R}, and β) are adjusted to reproduce the single-particle dynamics (see Fig. 1 in the SI).

In all experiments, particularly for $N = 4$ and $N = 5$, the system can evolve toward either dynamically fluctuating states or more stable configurations depending on the particles encountered within the trap. To control for this effect, a fixed initial configuration was imposed, and each case was repeated over 10 independent realizations.

Particle trajectories are recorded using a standard cellphone camera and analyzed with custom Python routines to extract positions and orientations (see details in SI).

III. Comparison between experiments and simulations

We conduct numerical simulations to investigate the role of magnetic dipole interactions and confinement while keeping the activity fixed. In particular, the active force F_0 (and thus the particle speed) and the rotational diffusivity D_{R} are held constant, allowing us to isolate the effects of the magnetic moment m and the harmonic trap stiffness κ on the system dynamics.

We first compare experimental and numerical results for different particle numbers N = 2, 3, 4 and 5 in the regime of nondimensional numbers $\Lambda_1 \sim 10$, $\Lambda_2 \propto 10^{-1}N$ and $\Lambda_3 \propto 10^{-2}N$.

A. Particle trajectories

Fig. 2 shows representative trajectories, where simulations (left column) and experiments (right column) exhibit qualitatively similar behavior. For N = 2 and 3, particles form chain-like configurations, corresponding to metastable states previously reported for magnetic active particles.[43,48,49] These structures undergo persistent motion around the trap while maintaining a preferential tilted-radial orientation, this is reflected also through their spatial exploration measured as a radial distribution presented in SI S3 with sharp peaks at particle positions during simulations. This behavior reflects a balance between activity and confinement, consistent with climbing states reported in confined active systems.[24,25,27]

The last two rows of Fig. 2 reveal a qualitative change in the system dynamics for N = 4 and N = 5, where the behavior is no longer dominated by simple climbing configurations but by collective reorganization within the trap.[27]

In our experiments, particle–particle friction sometimes stabilizes these configurations, leading to longer-lived cluster states (see Videos S2). In contrast, in simulations, where such effects are neglected, the system remains in a dynamically evolving metastable regime, forming chains or rotating clusters in which these configurations emerge intermittently over short times (see Videos S3). A similar behavior is also observed in our experimental realizations (see Videos S4).

For the analysis of trajectories and physical quantities, we focus on the experimental realizations where a dynamically evolving metastable regime is observed for N = 4 and N = 5 (see Video S4), as these provide a well-defined reference state for characterizing the collective behavior.

For N = 4 and N = 5 [Fig. 2(e)–(h)], particle trajectories are concentrated near the trap center but do not collapse into a single compact structure (see spatial exploration in SI S3). Instead, particles repeatedly approach, separate, and reassemble, generating a dense set of trajectories that reflects a dynamically evolving metastable state.

This indicates that, as the number of particles increases, dipolar interactions become sufficiently strong to promote clustering. This can be understood in terms of the dimensionless ratio $\Lambda_2 = \mu_0 m^2/(\kappa\sigma^5)$, which quantifies the competition between dipolar interactions and confinement: as N increases, the effective dipolar torque scales proportionally with the number of neighbors, causing magnetic interactions to dominate over both confinement and self-alignment in determining the particle configurations, while activity still allows for continuous rearrangement. This behavior is qualitatively consistent with the analytical results of Canavello *et al.*[27] and Aranson *et al.*,[31] where particles with weak self-alignment (in our case larger $\Lambda_3 \propto N$) form radially polarized clusters at a finite distance from the trap center, and with the metastable magnetic cluster configurations previously reported for active particles.[48]

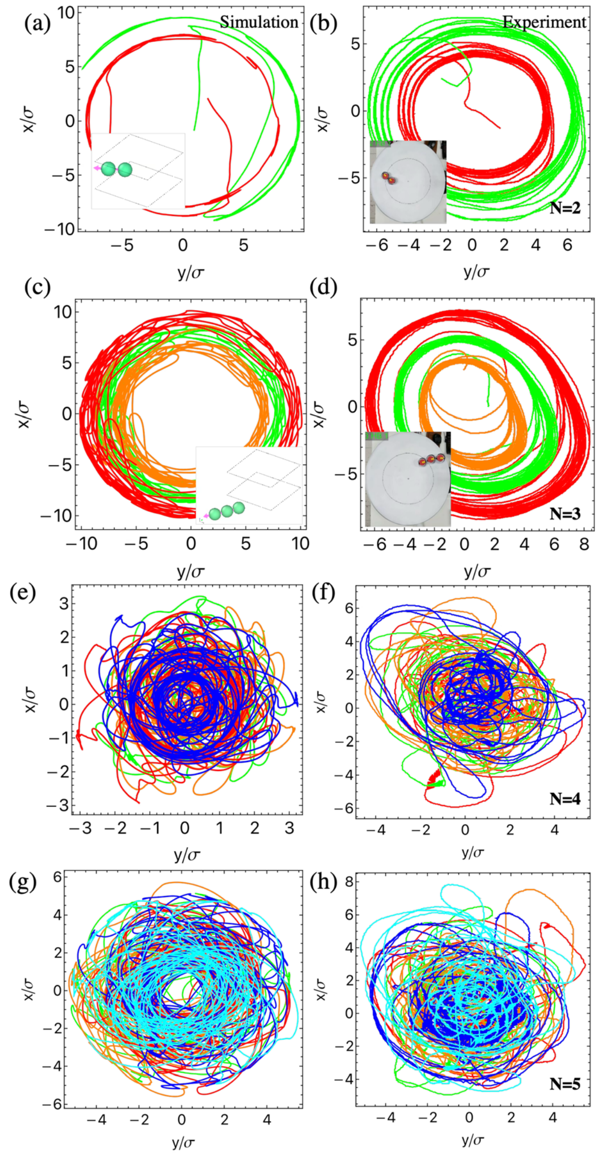

Fig. 2 Left column: Simulated trajectories illustrating persistent dynamical states for different particle numbers N. Insets show schematic representations of the corresponding steady configurations. Right column: Experimentally recorded trajectories of MSP-Hexbugs under comparable conditions. Insets display the steady configurations observed in each case. In some cases (*e.g.*, panels (e)–(h)), the dense trajectories reflect transient and dynamically evolving states, where particles continuously reorganize among metastable configurations rather than forming a single persistent structure.

B. Transient and steady states

Beyond particle trajectories and their spatial distributions, both experiments and simulations reveal a rich set of transient and steady configurations. These include chain-like structures, compact clusters, and vortex-like arrangements, which emerge dynamically from particle interactions. To quantify these behaviors, we analyze three time evolving quantities: the total magnetization, the velocity–orientation alignment, and the radius of gyration.

The total magnetization,

$$M_{\mathrm{T}} = \frac{1}{N}\left|\sum_{i=1}^{N} \hat{\mathbf{u}}_i\right|, \tag{6}$$

quantifies the degree of orientational order. Fig. 3 (left column) shows the time evolution of M_{T} for simulations (blue) and experiments (orange). A value $M_{\mathrm{T}} \approx 1$ corresponds to aligned configurations such as chains or polarized orbiting clusters, while $M_{\mathrm{T}} \approx 0$ is associated with rotating clusters or ring-like states.

For small particle numbers $N = 2, 3$, both experiments and simulations rapidly stabilize chain-like configurations, as observed in Fig. 3(a) and (b). Since $\Lambda_2 < 1$, confinement promotes particle encounters, while magnetic interactions stabilize chain configurations corresponding to metastable states previously reported for active magnetic particles.[48,49]

For $N = 4, 5$ [Fig. 3(c) and (d)], both experiments and simulations display intermittent fluctuations reflecting a dynamically evolving metastable regime, where magnetic torques and confinement compete to stabilize the system as $\Lambda_2 \sim 1$. Intervals where $M_{\mathrm{T}} \simeq 1$ correspond to polarized cluster configurations (see Fig. 4), similar to those observed experimentally, where clusters become more stable due to interparticle friction (see Video S2), and consistent with the weak self-alignment regime reported by Canavello *et al.*[27] In contrast, intervals where $M_{\mathrm{T}} \simeq 0$ correspond to rotating cluster configurations.

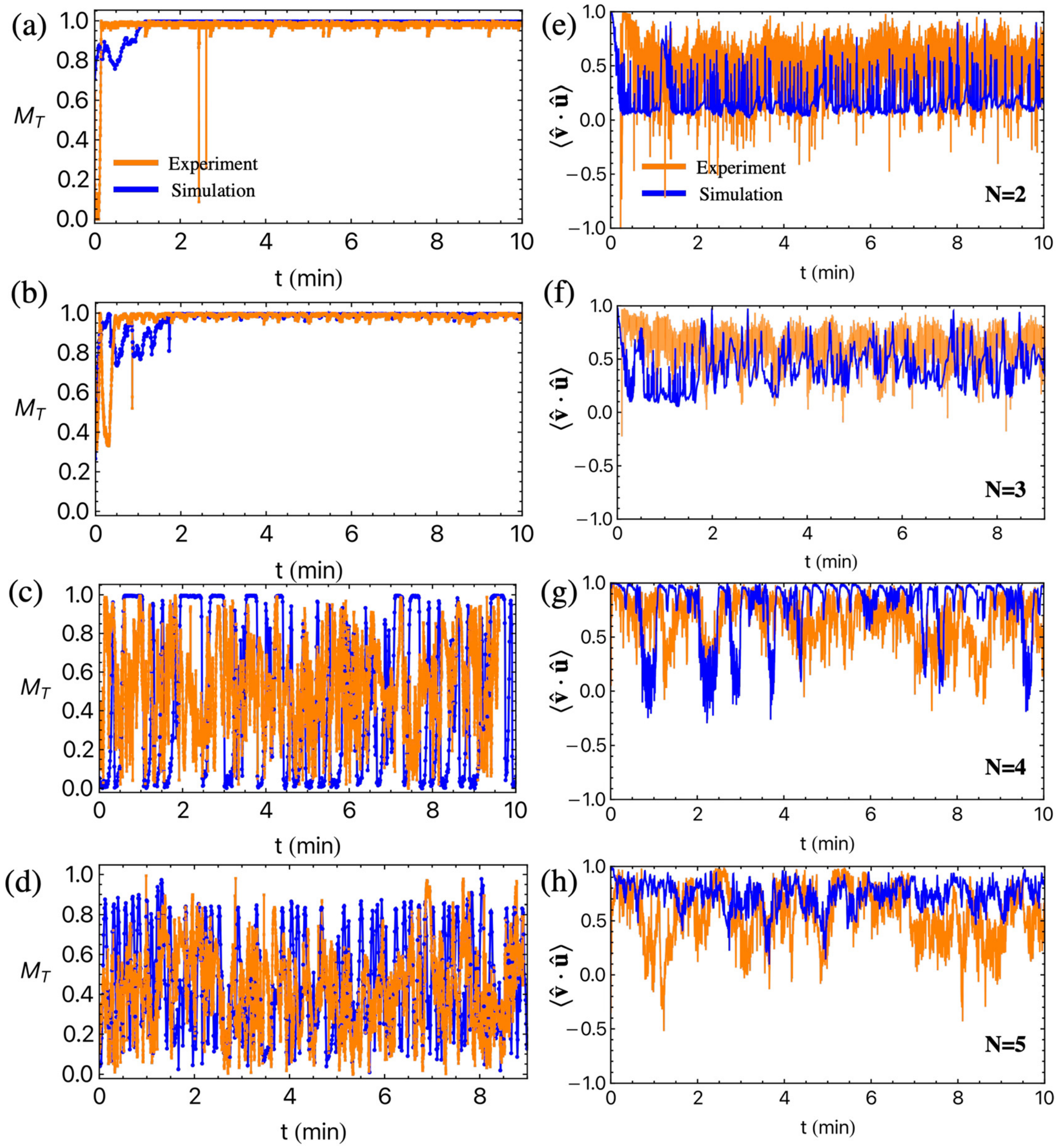

Fig. 3 Left column: (a)–(d) Time evolution of the total magnetization M_{T} for different particle numbers N. Simulations are shown in blue and experiments in orange. A value $M_{\mathrm{T}} \approx 1$ corresponds to aligned configurations such as chains or ferromagnetic clusters, while $M_{\mathrm{T}} \approx 0$ indicates rotating clusters or ring-like states. Right column: (e)–(h) Time evolution of the velocity orientation alignment $\langle \hat{\mathbf{v}} \cdot \hat{\mathbf{u}} \rangle$ for different particle numbers N. Simulations are shown in blue and experiments in orange.

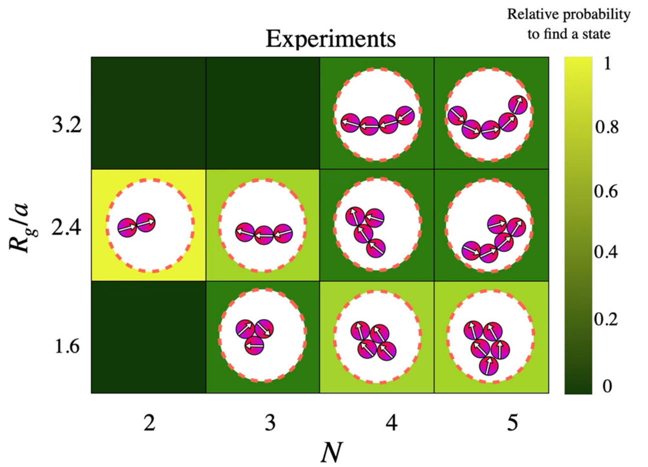

Fig. 4 Colormap of the relative probability of configurations as a function of the radius of gyration R_g/a for different particle numbers N (experiments). Lighter colors indicate more probable states. The system evolves from a single chain-like configuration at $N = 2$ to multiple coexisting metastable states for $N = 4$ and $N = 5$.

To further characterize these fluctuating states, we analyze the velocity–orientation alignment, defined as

$$\langle \hat{\mathbf{v}} \cdot \hat{\mathbf{u}} \rangle = \frac{1}{N}\sum_{i=1}^{N} \hat{\mathbf{v}}_i \cdot \hat{\mathbf{u}}_i, \tag{7}$$

which measures the degree of alignment between the instantaneous velocity and the propulsion direction of each particle. When particle motion occurs predominantly perpendicular to the orientation axis, $\langle \hat{\mathbf{v}}\cdot\hat{\mathbf{u}} \rangle \sim 0$, as in orbiting clusters where particles move tangentially while pointing radially. Conversely, $\langle \hat{\mathbf{v}}\cdot\hat{\mathbf{u}} \rangle \sim 1$ indicates that particles move along their propulsion direction, as in rotating ring configurations. This observable has been used similarly in[55] to characterize collective states in confined magnetic active matter. The time evolution of $\langle \hat{\mathbf{v}}\cdot\hat{\mathbf{u}} \rangle$is shown in Fig. 3 (right column).

For $N = 2, 3$, $\Lambda_3 \ll 1$, and the active torque associated with self-alignment still plays an important role over magnetic torque, as captured by the velocity–orientation alignment shown in Fig. 3(e) and (f) with $\langle \hat{\mathbf{v}}\cdot\hat{\mathbf{u}} \rangle \sim 0.5$. This indicates that particles within chain-like configurations are not fully aligned with their direction of motion. This behavior is consistent with the trajectories observed in the Videos and differs from the case of strong self-alignment, where one would expect particles to move tangentially along well-defined orbits with $\langle \hat{\mathbf{v}}\cdot\hat{\mathbf{u}} \rangle \sim 1$.[23,24,30] Moreover, $\langle \hat{\mathbf{v}}\cdot\hat{\mathbf{u}} \rangle$ slightly increases with particle number N (see Fig. 3(e) and (f)) as one would expect since $\Lambda_3 \propto N$ and the active torque associated with self-alignment becomes less dominant over magnetic torque.

However, as N increases, the system exhibits a broader range of dynamical behaviors, where particles continuously form, break, and reorganize into different configurations. In particular, transient clusters frequently appear and disassemble, leading to a complex dynamical landscape characterized by recurrent metastable states (see Movies S3 and S4). Since activity and confinement are fixed during both experiments and simulations, with $\Lambda_1 = 10$, the observed change in behavior for $N = 4$ and $N = 5$ (see Fig. 2 and 3) arises from the continuous variation of Λ_2 and Λ_3 with particle number.

For $N = 4, 5$, $\Lambda_2 \approx 1$, indicating that magnetic torques and confinement compete to determine the particle configurations, leading to states that are difficult to stabilize over time, as observed in Fig. 2(c) and (d). At the same time, $\Lambda_3 \propto 10^{-2}N$ increases, reducing the relative importance of self-alignment torques. This is reflected in the velocity-orientation alignment, which on average becomes closer to one, while still exhibiting strong temporal fluctuations and reaching intervals where $\langle \hat{\mathbf{v}}\cdot\hat{\mathbf{u}} \rangle \approx 0$. These intervals indicate that particle motion becomes predominantly tangential, while particle orientations remain approximately radial, corresponding to orbiting-like clusters rotating around the trap center with a misalignment between propulsion direction and actual motion.

Fig. 4 shows the relative probability of observing configurations characterized by their radius of gyration during experiments, defined as

$$R_g{}^2 = \frac{1}{N}\sum_{i=1}^{N}(\mathbf{r}_i - \mathbf{r}_{cm})^2, \tag{8}$$

where $\mathbf{r}_{cm}$ is the center of mass of the system. This quantity measures the spatial extent of particle configurations, allowing us to distinguish between compact clusters (small R_g) and more extended arrangements (large R_g).

For $N = 2$, the distribution is dominated by a single chain-like configuration. For $N = 3$, two states emerge, corresponding to a chain and a rotating cluster near the trap center, with the chain configuration being more likely to be observed than the ring-like configuration.

For $N = 4$ and $N = 5$, the relative probability to find a state broaden, reflecting the coexistence of multiple metastable configurations, including chain-like structures and polarized clusters. In both cases, polarized clusters are more likely to be observed. A direct comparison of the time evolution of the radius of gyration between simulations and experiments is presented in the SI S6.

Finally, to further elucidate the origin of these behaviors, we analyze in the SI the deterministic limit, where orientational noise is suppressed. In this regime, dynamical states persist even in the absence of rotatory diffusion. For $N = 2$, particles form a stable chain-like configuration. For $N = 3$, a dynamical state emerges in which one particle intermittently joins and leaves a chain. For $N = 4$, particles organize into two chain-like pairs oriented radially outward in opposite directions. For $N = 5$, the system exhibits a dynamically evolving state where particles follow each other and rotate collectively without reaching a fully ordered configuration. These results indicate that the observed dynamics is an intrinsic consequence of the interplay between interactions and confinement, rather than being solely induced by noise. While confinement tends to localize particles, dipolar interactions promote aggregation, and activity drives continuous reorganization. As a result, the system does not converge to a single equilibrium configuration, but instead explores a set of dynamically accessible states.

IV. Exploration of parameter space by simulation

We next explore the system behavior beyond the experimental parameters by varying κ and m in simulations while keeping the activity fixed. Fig. 5 shows the radial distributions for $N = 5$ under different combinations of confinement strength and magnetic interactions. Four distinct regimes emerge from the competition between dipolar interactions and harmonic confinement.

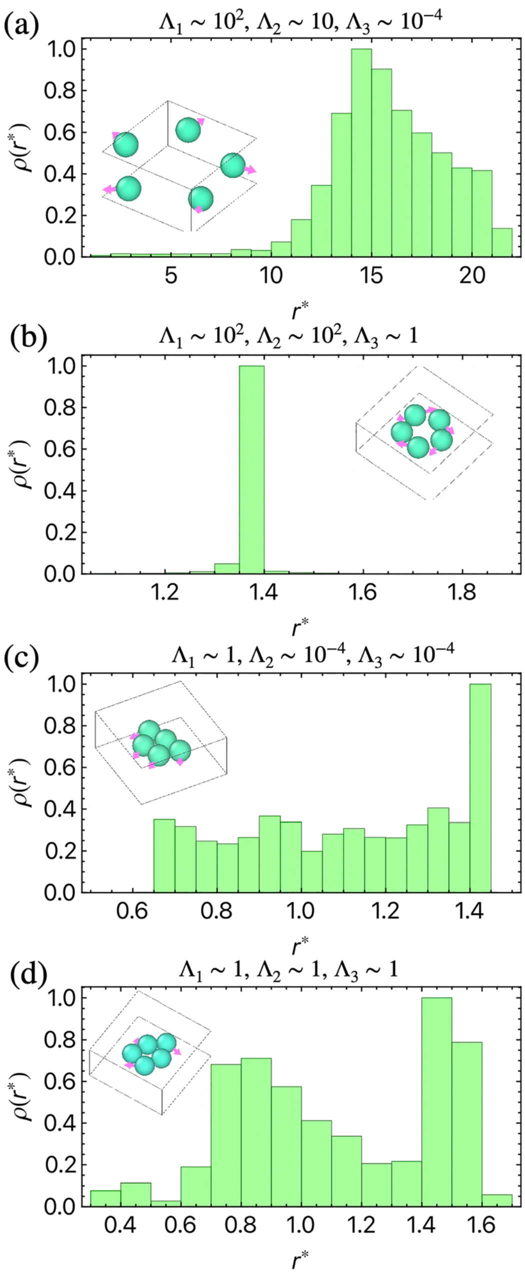

Fig. 5 Radial distributions $\rho(r^*)$ for $N = 5$ MSPPs under different values of the harmonic trap strength κ and magnetic dipole interaction m. The shape of the distributions reflects the emergence of different collective states, from (a) weakly interacting configurations to (b)–(d) compact, rotating clusters localized near the trap center. Insets display representative snapshots of the corresponding particle configurations for each case.

Using the parameter ranges explored in the simulations, these regimes can be interpreted in terms of the dimensionless ratios Λ_1, Λ_2 and Λ_3, which quantify the relative importance of activity *versus* confinement, dipolar interactions *versus* confinement and dipolar interactions and dipolar interactions *versus* active self-alignment torque, respectively. Varying κ and m allows us to span from weak to strong confinement and from weak to strong dipolar interactions.

For large Λ_1, activity overcomes confinement, allowing particles to explore large regions of the trap. If magnetic interactions are also weak, $\Lambda_2 \ll 1$, this leads to broad radial distributions (Fig. 5(a)). In this regime, both confinement and dipolar interactions are weak compared to activity, and the system remains highly dynamic without forming stable collective structures. Particle orientations tend to align radially with respect to the trap, consistent with previous observations for active particles in harmonic potentials.[20,27,29,30]

Increasing the magnetic moment under weak confinement (increasing Λ_3 while maintaining Λ_1 fixed) leads to a sharply peaked distribution at small radii, corresponding to the formation of a compact rotating cluster near the trap center. Here, dipolar interactions are dominant; this, combined with large activity $\Lambda_1 \gg 1$, stabilizes rotating rings (Fig. 5(b)).

Under strong confinement and weak magnetic interactions ($\Lambda_1 \sim 1$, Λ_2 small and Λ_3 small), particles form a compact cluster localized at a finite distance from the trap center. The narrow radial distribution reflects the persistence of this configuration. Within the cluste, particles tend to align approximately in the same direction, giving rise to a ferromagnetic-like state that undergoes coherent rotational motion around the trap, consistent with orbiting clusters reported in confined active systems[27] with weak self-alignment (Fig. 5(c)).

Finally, in the regime of strong confinement and strong dipolar interactions ($\Lambda_1 \sim 1$, $\Lambda_2 \sim 1$ and $\Lambda_3 \sim 1$), particles form a compact cluster localized near the trap center. This cluster undergoes coherent rotational motion while particle orientations continuously reorganize, maintaining a collectively ordered state. As a result, the radial distribution becomes center close to the harmonic trap center (Fig. 5(d)).

These results show that particle spatial organization is governed by the competition between dipolar interactions and harmonic confinement, while activity sets the overall scale of motion. The interplay between these effects gives rise to a range of metastable and dynamically evolving configurations, whose signatures are encoded in the radial distributions.

Importantly, the dynamical states observed here are not a direct consequence of self-alignment alone. As shown in the SI S4, increasing the self-alignment strength β promotes orbiting states characteristic of alignment-dominated dynamics. In contrast, for the weak self-alignment considered in the main text, the observed behavior is primarily governed by dipolar interactions, with confinement enhancing particle encounters and stabilizing magnetic-driven configurations.

V. Conclusions

In this work, we investigated the collective dynamics of magnetic self-propelled particles (MSPPs) confined in a harmonic potential, combining experiments and numerical simulations. The observed behavior emerges from the competition between activity, dipolar interactions, and confinement.

A central result is that self-alignment, which plays a key role in the single-particle dynamics,[23,24] does not determine the collective behavior when multiple particles interact through magnetic dipole forces. For a single particle, self-alignment promotes the orbiting state. However, once interactions are introduced, this single-particle orbiting behavior is less dominant as the particle number N increases.

Instead, for $N > 1$, confinement repeatedly promotes particle encounters, while dipolar interactions stabilize collective configurations, leading to the formation of chains, compact structures, and rotating clusters. These many-body states retain signatures of radially polarized (climbing-like) configurations, consistent with the small self-alignment regime reported in ref. 24 and 27. However, in contrast to the single-particle case, the collective dynamics is no longer governed by self-alignment, but by the interplay between dipolar interactions and confinement.

By varying the magnetic interaction strength and the confinement in simulations, we identify distinct dynamical regimes ranging from spatially extended configurations to compact and organized collective states. These results provide a consistent interpretation of the experimental observations and clarify how collective behavior emerges from the competition between dipolar interactions, confinement, and activity.

Beyond the identification of these configurations, we show that for N = 4,5 the system remains intrinsically dynamical, continuously reorganizing between metastable states. The persistence of these dynamics in the deterministic limit demonstrates that the observed behavior is not fluctuation-driven, but rather an inherent consequence of the nonlinear interplay between dipolar interactions, confinement, and activity. As a result, the system does not converge toward a single equilibrium configuration, but instead explores a landscape of dynamically accessible collective states.

Finally, we identify that as N increases cluster configurations, including ring-like states, emerge in the many-body regime. These states, together with the observed dynamical transitions, reveal how collective behavior in confined active systems with dipolar interactions depends on particle number and connects with previously reported orbiting cluster states in confined active systems.[27,31]

Our results establish that the collective behavior of confined magnetic active particles is governed by interaction-driven mechanisms, leading to a transition from alignment-dominated single-particle motion to complex, dynamically evolving many-body states controlled by dipolar interactions and confinement.

Author contributions

All authors contributed equally analyzing the data, and writing the manuscript; F. G.-L and H. L. propose the research, F. G.-L. performed the simulations. E. B lead the experiments. P. M. O, O. G and D. R performed the experiments. O. G. programmed the codes to analyze the experimental data.

Conflicts of interest

There are no conflicts to declare.

Acknowledgements

P. M. O., O. G., D. R. and F. G.-L. have received support from the ANID Millennium Science Initiative Program NCN19 170, Chile. F. G.-L. was supported by Fondecyt Iniciacin No. 11220683. F. G.-L. and H. L. thanks the support of DAAD award 91751172.

References

1 G. Gompper, R. G. Winkler, T. Speck, A. Solon, C. Nardini, F. Peruani, H. Löwen, R. Golestanian, U. B. Kaupp and L. Alvarez, *et al.*, The 2020 motile active matter roadmap, *J. Phys.: Condens. Matter*, 2020, **32**(19), 193001.
2 P. Romanczuk, M. Bär, W. Ebeling, B. Lindner and L. Schimansky-Geier, Active brownian particles: From individual to collective stochastic dynamics, *Eur. Phys. J.: Spec. Top.*, 2012, **202**, 1–162.
3 C. Bechinger, R. D. Leonardo, H. Löwen, C. Reichhardt, G. Volpe and G. Volpe, Active particles in complex and crowded environments, *Rev. Mod. Phys.*, 2016, **88**(4), 045006.
4 M. te Vrugt, B. Liebchen and M. E. Cates, What exactly is' active matter'? *arXiv*, 2025, preprint, arXiv:2507.21621, DOI: 10.48550/arXiv.2507.21621.
5 D. Chaudhuri, Active brownian particles: Entropy production and fluctuation response, *Phys. Rev. E: Stat., Nonlinear, Soft Matter Phys.*, 2014, **90**(2), 022131.
6 O. Pohl and H. Stark, Dynamic clustering and chemotactic collapse of self-phoretic active particles, *Phys. Rev. Lett.*, 2014, **112**(23), 238303.
7 N. Vanesse, E. Opsomer, G. Lumay and N. Vandewalle, Collective dynamics of dipolar self-propelled particles, *Phys. Rev. E*, 2023, **108**(2), 024608.
8 A. Filella, F. Nadal, C. Sire, E. Kanso and C. Eloy, Model of collective fish behavior with hydrodynamic interactions, *Phys. Rev. Lett.*, 2018, **120**(19), 198101.
9 A. Petroff, A. Rosselli-Calderon, B. Roque and P. Kumar, Phases of active matter composed of multicellular magnetotactic bacteria near a hard surface, *Phys. Rev. Fluids*, 2022, **7**(5), 053102.
10 M. E. Cates, Diffusive transport without detailed balance in motile bacteria: does microbiology need statistical physics?, *Rep. Prog. Phys.*, 2012, **75**(4), 042601.
11 J. P. Carrillo-Mora, A. Garcés and D. Levis, Depinning and activated motion of chiral self-propelled robots, *arXiv*,

2025, preprint, arXiv:2506.20610, DOI: 10.48550/arXiv.2506.20610.
12 A. Deblais, T. Barois, T. Guerin, P.-H. Delville, R. Vaudaine, J. S. Lintuvuori, J.-F. Boudet, J.-C. Baret and H. Kellay, Boundaries control collective dynamics of inertial self-propelled robots, *Phys. Rev. Lett.*, 2018, **120**(18), 188002.
13 L. Giomi, N. Hawley-Weld and L. Mahadevan, Swarming, swirling and stasis in sequestered bristle-bots, *Proc. R. Soc. A*, 2013, **469**(2151), 20120637.
14 H. R. Vutukuri, B. Bet, R. Van Roij, M. Dijkstra and W. T. S. Huck, Rational design and dynamics of self-propelled colloidal bead chains: from rotators to flagella, *Sci. Rep.*, 2017, **7**(1), 16758.
15 N. A. M. Araújo, L. M. C. Janssen, T. Barois, G. Boffetta, I. Cohen, A. Corbetta, O. Dauchot, M. Dijkstra, W. M. Durham and A. Dussutour, *et al.*, Steering self-organisation through confinement, *Soft Matter*, 2023, **19**(9), 1695–1704.
16 U. Basu, S. N. Majumdar, A. Rosso and G. Schehr, Active brownian motion in two dimensions, *Phys. Rev. E*, 2018, **98**(6), 062121.
17 T. Faúndez, B. Espinoza, R. Soto and F. Guzmán-Lastra., Microbial adhesion on circular obstacles: An optimization study, *Front. Phys.*, 2022, **10**, 865937.
18 F. Ginot, I. Theurkauff, D. Levis, C. Ybert, L. Bocquet, L. Berthier and C. Cottin-Bizonne, Nonequilibrium equation of state in suspensions of active colloids, *Phys. Rev. X*, 2015, **5**(1), 011004.
19 M. Leoni, M. Paoluzzi, S. Eldeen, A. Estrada, L. Nguyen, M. Alexandrescu, K. Sherb and W. W. Ahmed, Surfing and crawling macroscopic active particles under strong confinement: Inertial dynamics, *Phys. Rev. Res.*, 2020, **2**(4), 043299.
20 M. Caraglio and T. Franosch, Analytic solution of an active brownian particle in a harmonic well, *Phys. Rev. Lett.*, 2022, **129**(15), 158001.
21 S. Jahanshahi, H. Löwen and B. T. Hagen, Brownian motion of a circle swimmer in a harmonic trap, *Phys. Rev. E*, 2017, **95**(2), 022606.
22 S. C. Takatori, R. De Dier, J. Vermant and J. F. Brady, Acoustic trapping of active matter, *Nat. Commun.*, 2016, **7**(1), 10694.
23 C. Tapia-Ignacio, L. L. Gutierrez-Martinez and M. Sandoval., Trapped active toy robots: theory and experiment, *J. Stat. Mech.: Theory Exp.*, 2021, **5**, 053404.
24 O. Dauchot and V. Démery, Dynamics of a self-propelled particle in a harmonic trap, *Phys. Rev. Lett.*, 2019, **122**(6), 068002.
25 R. H. Damascena, L. Re Cabral and C. C. de Souza Silva, Coexisting orbits and chaotic dynamics of a confined self-propelled particle, *Phys. Rev. E*, 2022, **105**(6), 064608.
26 R. H. Damascena and Clécio C. de S. Silva, Noise-induced escape of a self-propelled particle from metastable orbits, *Phys. Rev. E*, 2023, **108**(4), 044605.
27 D. Canavello, R. H. Damascena, L. R. E. Cabral and C. C. de S. Silva, Polar order, shear banding, and clustering in confined active matter, *Soft Matter*, 2024, **20**(10), 2310–2320.
28 P. Baconnier, O. Dauchot, V. Démery, G. Düring, S. Henkes, C. Huepe and A. Shee, Self-aligning polar active matter, *Rev. Mod. Phys.*, 2025, **97**(1), 015007.
29 I. Buttinoni, L. Caprini, L. Alvarez, F. Jan Schwarzendahl and H. Löwen, Active colloids in harmonic optical potentials (a), *Europhys. Lett.*, 2022, **140**(2), 27001.
30 L. L. Gutierrez-Martinez and M. Sandoval, Inertial effects on trapped active matter, *J. Chem. Phys.*, 2020, **153**(4), 044906.
31 I. S. Aranson and A. Pikovsky, Confinement and collective escape of active particles, *Phys. Rev. Lett.*, 2022, **128**(10), 108001.
32 R. Messina, L. A. Khalil and I. Stanković., Self-assembly of magnetic balls: From chains to tubes, *Phys. Rev. E: Stat., Nonlinear, Soft Matter Phys.*, 2014, **89**(1), 011202.
33 S. Klumpp, C. T. Lefèvre, M. Bennet and D. Faivre, Swimming with magnets: from biological organisms to synthetic devices, *Phys. Rep.*, 2019, **789**, 1–54.
34 B. Vincenti, G. Ramos, M. Luisa Cordero, C. Douarche, R. Soto and E. Clement, Magnetotactic bacteria in a droplet self-assemble into a rotary motor, *Nat. Commun.*, 2019, **10**(1), 5082.
35 H. Lee, A. M. Purdon, V. Chu and R. M. Westervelt, Controlled assembly of magnetic nanoparticles from magnetotactic bacteria using microelectromagnets arrays, *Nano Lett.*, 2004, **4**(5), 995–998.
36 N. Waisbord, C. T. Lefèvre, L. Bocquet, C. Ybert and C. Cottin-Bizonne, Destabilization of a flow focused suspension of magnetotactic bacteria, *Phys. Rev. Fluids*, 2016, **1**(5), 053203.
37 A. Théry, L. Le Nagard, J.-C. Ono-dit Biot, C. Fradin, K. Dalnoki-Veress and E. Lauga, Self-organisation and convection of confined magnetotactic bacteria, *Sci. Rep.*, 2020, **10**, 13578.
38 R. Dreyfus, J. Baudry, M. L. Roper, M. Fermigier, H. A. Stone and J. Bibette, Microscopic artificial swimmers, *Nature*, 2005, **437**(7060), 862–865.
39 F. Martinez-Pedrero, A. Ortiz-Ambriz, I. Pagonabarraga and P. Tierno, Colloidal microworms propelling via a cooperative hydrodynamic conveyor belt, *Phys. Rev. Lett.*, 2015, **115**(13), 138301.
40 P. Tierno, R. Golestanian, I. Pagonabarraga and F. Sagués, Magnetically actuated colloidal microswimmers, *J. Phys. Chem. B*, 2008, **112**(51), 16525–16528.
41 G.-J. Liao, C. K. Hall and S. H. L. Klapp, Dynamical self-assembly of dipolar active brownian particles in two dimensions, *Soft Matter*, 2020, **16**(9), 2208–2223.
42 G.-J. Liao and S. H. L. Klapp, Emergent vortices and phase separation in systems of chiral active particles with dipolar interactions, *Soft Matter*, 2021, **17**(28), 6833–6847.
43 V. Telezki and S. Klumpp, Simulations of structure formation by confined dipolar active particles, *Soft Matter*, 2020, **16**(46), 10537–10547.
44 F. Kogler and S. H. L. Klapp, Lane formation in a system of dipolar microswimmers, *Europhys. Lett.*, 2015, **110**(1), 10004.
45 T. Vicsek, A. Czirók, E. Ben-Jacob, I. Cohen and O. Shochet, Novel type of phase transition in a system of self-driven particles, *Phys. Rev. Lett.*, 1995, **75**(6), 1226.
46 H. Xie, M. Sun, X. Fan, Z. Lin, W. Chen, L. Wang, L. Dong and Q. He, Reconfigurable magnetic microrobot swarm:

Multimode transformation, locomotion, and manipulation, *Sci. Rob.*, 2019, **4**(28), eaav8006.
47 J. Yan, M. Han, J. Zhang, C. Xu, E. Luijten and S. Granick, Reconfiguring active particles by electrostatic imbalance, *Nat. Mater.*, 2016, **15**(10), 1095–1099.
48 F. Guzmán-Lastra, A. Kaiser and H. Löwen, Fission and fusion scenarios for magnetic microswimmer clusters, *Nat. Commun.*, 2016, **7**(1), 13519.
49 A. Kaiser, K. Popowa and H. Löwen, Active dipole clusters: From helical motion to fission, *Phys. Rev. E: Stat., Nonlinear, Soft Matter Phys.*, 2015, **92**(1), 012301.
50 Hexbug, Hexbug is a brand of toy automata developed and distributed by innovation first. https://www.hexbug.com/.
51 N. Sepúlveda, F. Guzmán-Lastra, M. Carrasco, B. González, E. Hamm and A. Concha, Bioinspired magnetic active matter and the physical limits of magnetotaxis, *arXiv*, 2021, preprint, arXiv:2111.04889, DOI: 10.48550/arXiv.2111.04889.
52 K. Engbring, D. Boriskovsky, Y. Roichman and B. Lindner, A nonlinear fluctuation-dissipation test for markovian systems, *Phys. Rev. X*, 2023, **13**(2), 021034.
53 S. Lévay, A. Katona, H. Löwen, R. Cruz Hidalgo and I. Zuriguel, Cluster dynamics in macroscopic photoactive particles, *Phys. Rev. Lett.*, 2025, **135**(9), 098301.
54 X. Yang, C. Ren, K. Cheng and H. P. Zhang, Robust boundary flow in chiral active fluid, *Phys. Rev. E*, 2020, **101**(2), 022603.
55 M. Musacchio, M. Felber, M. Paoluzzi, A. Gnoli, A. Puglisi and L. Angelani, Fluidization induced by magnetic interactions in confined active matter, *Phys. Rev. E*, 2026, **113**(5), 055413.
56 E. Zheng, M. Brandenbourger, L. Robinet, P. Schall, E. Lerner and C. Coulais, Self-oscillation and synchronization transitions in elastoactive structures, *Phys. Rev. Lett.*, 2023, **130**(17), 178202.